The Astrophysical Journal, 794:12 (14pp), 2014 October 10 doi:10.1088/0004-637X/794/1/12
© 2014. The American Astronomical Society. All rights reserved. Printed in the U.S.A.

SPT-CL J2040−4451: AN SZ-SELECTED GALAXY CLUSTER AT $z = 1.478$ WITH SIGNIFICANT ONGOING STAR FORMATION

M. B. Bayliss[1,2], M. L. N. Ashby[2], J. Ruel[1], M. Brodwin[3], K. A. Aird[4], M. W. Bautz[5], B. A. Benson[6,7], L. E. Bleem[6,8,9], S. Bocquet[10,11], J. E. Carlstrom[6,7,8,9,12], C. L. Chang[6,7,9], H. M. Cho[13], A. Clocchiatti[14], T. M. Crawford[6,12], A. T. Crites[6,12], S. Desai[10,11], M. A. Dobbs[15], J. P. Dudley[15], R. J. Foley[2,16,17], W. R. Forman[2], E. M. George[18], D. Gettings[19], M. D. Gladders[6,12], A. H. Gonzalez[19], T. de Haan[15], N. W. Halverson[20], F. W. High[6,12], G. P. Holder[15], W. L. Holzapfel[18], S. Hoover[6,7], J. D. Hrubes[4], C. Jones[2], M. Joy[21], R. Keisler[6,8], L. Knox[22], A. T. Lee[18,23], E. M. Leitch[6,12], J. Liu[10,11], M. Lueker[18,24], D. Luong-Van[4], A. Mantz[6], D. P. Marrone[25], K. Mawatari[2], M. McDonald[5,36], J. J. McMahon[26], J. Mehl[6,9,12], S. S. Meyer[6,7,8,12], E. D. Miller[5], L. Mocanu[6,12], J. J. Mohr[10,11,27], T. E. Montroy[28], S. S. Murray[2], S. Padin[6,12,24], T. Plagge[6,12], C. Pryke[29], C. L. Reichardt[18], A. Rest[30], J. E. Ruhl[28], B. R. Saliwanchik[28], A. Saro[10], J. T. Sayre[28], K. K. Schaffer[6,7,31], E. Shirokoff[18,24], J. Song[26], B. Stalder[2], R. Šuhada[10], H. G. Spieler[23], S. A. Stanford[22,32], Z. Staniszewski[28], A. A. Stark[2], K. Story[6,8], C. W. Stubbs[1,2], A. van Engelen[15], K. Vanderlinde[33,34], J. D. Vieira[6,8,16,17,24], A. Vikhlinin[2], R. Williamson[6,12], O. Zahn[18,35], and A. Zenteno[10,11]

[1] Department of Physics, Harvard University, 17 Oxford Street, Cambridge, MA 02138, USA; mbayliss@cfa.harvard.edu
[2] Harvard-Smithsonian Center for Astrophysics, 60 Garden Street, Cambridge, MA 02138, USA
[3] Department of Physics and Astronomy, University of Missouri, 5110 Rockhill Road, Kansas City, MO 64110, USA
[4] University of Chicago, 5640 South Ellis Avenue, Chicago, IL 60637, USA
[5] Kavli Institute for Astrophysics and Space Research, Massachusetts Institute of Technology, 77 Massachusetts Avenue, Cambridge, MA 02139, USA
[6] Kavli Institute for Cosmological Physics, University of Chicago, 5640 South Ellis Avenue, Chicago, IL 60637, USA
[7] Enrico Fermi Institute, University of Chicago, 5640 South Ellis Avenue, Chicago, IL 60637, USA
[8] Department of Physics, University of Chicago, 5640 South Ellis Avenue, Chicago, IL 60637, USA
[9] Argonne National Laboratory, 9700 S. Cass Avenue, Argonne, IL 60439, USA
[10] Department of Physics, Ludwig-Maximilians-Universität, Scheinerstr. 1, D-81679 München, Germany
[11] Excellence Cluster Universe, Boltzmannstr. 2, D-85748 Garching, Germany
[12] Department of Astronomy and Astrophysics, University of Chicago, 5640 South Ellis Avenue, Chicago, IL 60637, USA
[13] NIST Quantum Devices Group, 325 Broadway Mailcode 817.03, Boulder, CO 80305, USA
[14] Departamento de Astronomia y Astrosifica, Pontificia Universidad Catolica, Chile
[15] Department of Physics, McGill University, 3600 Rue University, Montreal, Quebec H3A 2T8, Canada
[16] Astronomy Department, University of Illinois at Urbana-Champaign, 1002 West Green Street, Urbana, IL 61801, USA
[17] Department of Physics, University of Illinois at Urbana-Champaign, 1110 West Green Street, Urbana, IL 61801, USA
[18] Department of Physics, University of California, Berkeley, CA 94720, USA
[19] Department of Astronomy, University of Florida, Gainesville, FL 32611, USA
[20] Department of Astrophysical and Planetary Sciences and Department of Physics, University of Colorado, Boulder, CO 80309, USA
[21] Department of Space Science, VP62, NASA Marshall Space Flight Center, Huntsville, AL 35812, USA
[22] Department of Physics, University of California, One Shields Avenue, Davis, CA 95616, USA
[23] Physics Division, Lawrence Berkeley National Laboratory, Berkeley, CA 94720, USA
[24] California Institute of Technology, 1200 E. California Blvd., Pasadena, CA 91125, USA
[25] Steward Observatory, University of Arizona, 933 North Cherry Avenue, Tucson, AZ 85721, USA
[26] Department of Physics, University of Michigan, 450 Church Street, Ann Arbor, MI 48109, USA
[27] Max-Planck-Institut für Extraterrestrische Physik, Giessenbachstr., D-85748 Garching, Germany
[28] Physics Department, Center for Education and Research in Cosmology and Astrophysics, Case Western Reserve University, Cleveland, OH 44106, USA
[29] Physics Department, University of Minnesota, 116 Church Street S.E., Minneapolis, MN 55455, USA
[30] Space Telescope Science Institute, 3700 San Martin Drive, Baltimore, MD 21218, USA
[31] Liberal Arts Department, School of the Art Institute of Chicago, 112 S. Michigan Avenue, Chicago, IL 60603, USA
[32] Institute of Geophysics and Planetary Physics, Lawrence Livermore National Laboratory, Livermore, CA 94551, USA
[33] Dunlap Institute for Astronomy and Astrophysics, University of Toronto, 50 St. George Street, Toronto, ON, M5S 3H4, Canada
[34] Department of Astronomy and Astrophysics, University of Toronto, 50 St. George St, Toronto, ON, M5S 3H4, Canada
[35] Berkeley Center for Cosmological Physics, Department of Physics, University of California, and Lawrence Berkeley National Labs, Berkeley, CA 94720, USA
Received 2013 July 9; accepted 2014 August 6; published 2014 September 18

ABSTRACT

SPT-CL J2040−4451—spectroscopically confirmed at $z = 1.478$—is the highest-redshift galaxy cluster yet discovered via the Sunyaev–Zel'dovich effect. SPT-CL J2040−4451 was a candidate galaxy cluster identified in the first 720 deg^2 of the South Pole Telescope Sunyaev–Zel'dovich (SPT-SZ) survey, and has been confirmed in follow-up imaging and spectroscopy. From multi-object spectroscopy with Magellan-I/Baade+IMACS we measure spectroscopic redshifts for 15 cluster member galaxies, all of which have strong [O II] λλ3727 emission. SPT-CL J2040−4451 has an SZ-measured mass of $M_{500,\mathrm{SZ}} = 3.2 \pm 0.8 \times 10^{14}\, M_\odot\, h_{70}^{-1}$, corresponding to $M_{200,\mathrm{SZ}} = 5.8 \pm 1.4 \times 10^{14}\, M_\odot\, h_{70}^{-1}$. The velocity dispersion measured entirely from blue star-forming members is $\sigma_v = 1500 \pm 520\,\mathrm{km\,s^{-1}}$. The prevalence of star-forming cluster members (galaxies with $>1.5\, M_\odot\,\mathrm{yr}^{-1}$) implies that this massive, high-redshift cluster is experiencing a phase of active star formation, and supports recent results showing a marked increase in star formation occurring in galaxy clusters at $z \gtrsim 1.4$. We also compute the probability of

finding a cluster as rare as this in the SPT-SZ survey to be >99%, indicating that its discovery is not in tension with the concordance ΛCDM cosmological model.

Key words: galaxies: clusters: individual (SPT-CL J2040−4451) – galaxies: distances and redshifts – galaxies: evolution – large-scale structure of universe

Online-only material: color figures

1. INTRODUCTION

As the most massive collapsed structures in the universe, galaxy clusters are both a sensitive probe of cosmology and an extreme environment for studying galaxy evolution. Specifically, galaxy clusters are the most over-dense environments in the universe and provide a laboratory for constraining the astrophysics of how galaxies form stars and evolve (e.g., Oemler 1974; Dressler 1980; Dressler & Gunn 1983; Balogh et al. 1997; Blanton & Moustakas 2009). Massive galaxy clusters evolve from the most extreme peaks of the initial cosmic matter distribution, and until recently there was a consensus in the literature that the galaxies in clusters formed during a short-lived burst of star formation at early times ($z \gtrsim 3$) before quickly settling into a stable mode of passive evolution (Stanford et al. 1998, 2005; Holden et al. 2005; Mei et al. 2006). However, recent studies of clusters at $z > 1$ have begun to reveal evidence for an era of active star formation and evolution of the cluster luminosity function (LF) at $z \gtrsim 1.4$ (Hilton et al. 2009; Mancone et al. 2010, 2012; Tran et al. 2010; Fassbender et al. 2011; Snyder et al. 2012; Zeimann et al. 2012; Brodwin et al. 2013), suggesting that clusters in this epoch of the universe are undergoing a phase of significant galaxy assembly.

The high-redshift frontier for both cosmological and astrophysical studies of galaxy clusters is now extended well beyond $z \gtrsim 1$, where large, well-defined samples of galaxy clusters have only recently begun to emerge. Several groups have had success identifying high-redshift galaxy clusters using deep observations at X-ray (e.g., Rosati et al. 2004, 2009; Mullis et al. 2005; Stanford et al. 2006) and optical+near infrared (NIR) wavelengths (e.g., Stanford et al. 2005, 2012; Brodwin et al. 2006, 2011; Elston et al. 2006; Eisenhardt et al. 2008; Muzzin et al. 2009; Papovich et al. 2010; Santos et al. 2011; Gettings et al. 2012; Zeimann et al. 2012), but exploration of this high-redshift frontier has proven challenging. The challenge arises because observable signatures that are commonly used for cluster detection (e.g., X-ray and optical flux) diminish toward high redshift, and also because massive clusters become increasingly rare earlier in the universe.

Recent years have seen the emergence of a new generation of dedicated surveys that identify massive galaxy clusters via the Sunyaev–Zel'dovich (SZ) Effect. Several SZ galaxy cluster surveys are underway; the *Planck* satellite (Planck Collaboration et al. 2013), the Atacama Cosmology Telescope (ACT; Marriage et al. 2011; Hasselfield et al. 2013), and the South Pole Telescope (SPT; Staniszewski et al. 2009; Vanderlinde et al. 2010; Williamson et al. 2011; Reichardt et al. 2013) have all produced SZ galaxy cluster catalogs. SZ Effect surveys with sufficient angular resolution to resolve galaxy clusters on the sky (e.g., ACT and SPT) benefit from an approximately flat selection in mass beyond $z \gtrsim 0.3$ (Carlstrom et al. 2002), which results in samples with a clean selection extending into the $z > 1$ universe. From the first 720 (of 2500) deg^2 of the SPT-SZ survey, 10 clusters have been confirmed (regarding the meaning of "confirmed"; see Song et al. 2012) at $z > 1$, including Six spectroscopically (Brodwin et al. 2010; Foley et al. 2011; Stalder et al. 2013; Song et al. 2012; Reichardt et al. 2013; Ruel et al. 2014). In this work we present spectroscopic observations of the highest-redshift cluster in the first 720 deg^2 of the SPT-SZ survey. SPT-CL J2040−4451 is the most distant galaxy cluster yet discovered via the SZ effect, the second most distant cluster with an SZ measurement after IDCS J1426.5+3508 ($z = 1.75$, $M_{200} = 4.3 \pm 1.1 \times 10^{14}\ M_\odot$; Brodwin et al. 2012), and one of only a few spectroscopically confirmed galaxy clusters currently known at $z > 1.4$.

This paper is organized as follows. In Section 2 we describe the observations that were critical to the work presented and their reduction. In Section 3 we identify spectroscopically confirmed galaxy members in SPT-CL J2040−4451, and report their star formation rates (SFRs), along with the mass and dynamics of the cluster. In Section 4 we discuss the properties of the spectroscopic cluster members in color–magnitude space, and explore the implications of the high incidence of star formation among the cluster members. Finally, we briefly summarize our results in Section 5. Throughout this paper we present magnitudes calibrated relative to Vega, and calculate cosmological values assuming a standard flat cold dark matter with a cosmological constant (ΛCDM) cosmology with $H_0 = 70$ km s^{-1} Mpc^{-1}, and matter density $\Omega_M = 0.27$ (Komatsu et al. 2011).

2. OBSERVATIONS AND DATA

2.1. Millimeter Observations by the South Pole Telescope

The SPT-SZ survey (Carlstrom et al. 2011) finished in 2011 November, and covered 2500 deg^2 at observing frequencies of 95, 150, and 220 GHz to approximate depths of 40′, 18′, and 70′μK, respectively. Clusters are identified in the SPT-SZ survey via the SZ effect, the inverse Compton scattering of cosmic microwave background (CMB) photons off of hot intra-cluster gas (Sunyaev & Zel'dovich 1972). The selection threshold of the SPT-SZ survey is expected to fall slightly in mass with increasing redshift, and the resulting cluster sample is predicted to be ∼100% complete at $z > 0.3$ for a mass threshold of $M_{500} \gtrsim 5 \times 10^{14}\ M_\odot\ h_{70}^{-1}$, and at $z > 1.0$ for a mass threshold of $M_{500} \gtrsim 3 \times 10^{14}\ M_\odot\ h_{70}^{-1}$. Details regarding the survey strategy and data analysis are detailed in the previous SPT-SZ survey papers (Staniszewski et al. 2009; Vanderlinde et al. 2010; Williamson et al. 2011; Reichardt et al. 2013).

SPT-CL J2040−4451 was initially discovered in the first 720 deg^2 of the SPT-SZ survey and reported in Reichardt et al. (2013). It was measured to have a SPT detection significance, ξ, of 6.28, where ξ is a statistic that reports the strength of the detection of the SZ decrement and scales monotonically with mass. The SPT detection is centered at $(\alpha, \delta) = (20{:}40{:}59.23, -44{:}51{:}35.6)$ (J2000.0), and an image of the filtered SPT map is shown in Figure 1. In Section 3.3, we report a new SZ mass

[36] Hubble Fellow.

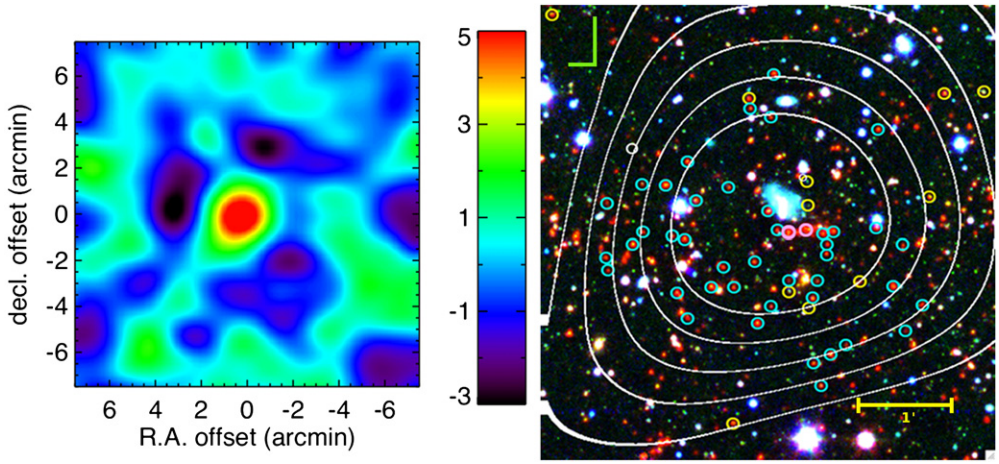

Figure 1. Left: the filtered SPT-SZ significance map of SPT-CL J2040−4451 with a color map indicating significance, ξ. The negative trough surrounding the cluster is an artifact of the filtering of the time ordered data and maps. Right: color image of the $4' \times 4'$ central region around SPT-CL J2040−4451 from *Spitzer*/IRAC [3.6] (red) plus Megacam i' (green), and MOSAIC-II r band (blue) with the SPT-SZ contours over-plotted in white. Photometrically selected cluster members are identified with cyan circles, while spectroscopically confirmed cluster members are identified with yellow circles. The two candidate brightest cluster galaxies (BCGs) are indicated by magenta circles, located near the centroid of the SZ signal. The bright blue extended source located near the center of the SZ contours is an intervening foreground galaxy. North and east are indicated by the green axes in the upper left corner, with north being the longer axis.

(A color version of this figure is available in the online journal.)

estimate based on its measured SPT significance and our updated redshift measurement since Reichardt et al. (2013).

2.2. Optical and Infrared Imaging

We obtained gri imaging using the MOSAIC-II imager on the CTIO 4 m Blanco Telescope on UT 2010 October 29 and z imaging on UT 2011 November 3. Both nights were clear, with seeing of $\sim 1''.35$ in the 2010 October runs, and $0''.68$ in the z-band data taken in 2011 November. Total integration times were 750, 1200, 1347, and 2400 s in g, r, i, and z, to 10σ point source depths of 23.5, 22.6, 21.6, and 21.2 mag (Vega) in g, r, i, and z, respectively. The MOSAIC-II data were reduced using the PHOTPIPE pipeline (Rest et al. 2005), and calibrated photometrically using the stellar locus regression technique of High et al. (2009).

We also obtained deep follow-up imaging in i' with the Megacam imager (McLeod et al. 2006) on the 6.5 m Clay Magellan Telescope on 2012 October 24. These observations consist of 9×200 s dithered exposures. The exposures were taken in seeing ranging from $0''.7$ to $0''.9$, through variable thin cirrus clouds. The Megacam data were reduced at the Harvard-Smithsonian Center for Astrophysics with a custom-designed pipeline in addition to standard IRAF/mscred routines. After implementing pointing refinements, the nine i' exposures were co-added to produce a final mosaic with an effective FWHM of $0''.82$. We calibrate photometry from the final Megacam i' mosaic by matching hundreds of well-detected, unsaturated objects that are also detected in the MOSAIC-II i-band imaging described above; this calibration includes a color term that accounts for the different throughput curves of the MOSAIC-II i and Megacam i' filters.

Further ground-based NIR imaging was obtained for SPT-CL J2040−4451 from two different facilities. K_s imaging with the NEWFIRM imager (Autry et al. 2003) at the CTIO 4 m Blanco Telescope was obtained on UT 2011 July 14. Conditions during the observations were intermittently cloud with highly variable seeing. The K_s observations consist of 60 s exposures divided among 6 co-adds in a 16 point dither pattern, and were reduced with the FATBOY pipeline modified to work with NEWFIRM data in support of the Infrared Bootes Imaging Survey from the original version developed for the FLAMINGOS-2 instrument (Gonzalez et al. 2010). SCAMP and SWarp were used to combine individual processed frames. Additionally, J-band imaging with Magellan/Baade+Fourstar was collected on UT 2012 June 10 and 11 in photometric conditions. A total of 30×32 s exposures were taken at 15 different pointed positions centered on the coordinates of the cluster. The images were flat-fielded using standard IRAF routines; World Coordinate System (WCS) registering and stacking were done using the PHOTPIPE pipeline. The final J and K_s images were calibrated photometrically to Two Micron All Sky Survey (Skrutskie et al. 2006), and have FWHM of $0''.58$ and $2''.6$ in J and K_s, respectively.

Infrared imaging for SPT-CL J2040−4451 was acquired in 2011 with *Spitzer*/IRAC (Fazio et al. 2004) as a part of a larger *Spitzer* Cycle 7 effort to follow up clusters identified in the SPT survey. The on-target observations consisted of 8×100 s and 6×30 s dithered exposures in bands [3.6] and [4.5], reaching 10σ depths of 20.3 and 18.8 mag, respectively, with an effective spatial FWHM of $\sim 1''.66$. The [3.6] observations are sensitive to passively evolving cluster galaxies down to 0.1 L^* at $z = 1.5$. The data reduction is identical to that in Brodwin et al. (2010), applying the method of Ashby et al. (2009). All imaging observations are summarized in Table 1, and we show an IRAC+optical+SZ contour image of the core of SPT-CL J2040−4451 in Figure 1. The red sequence excess of galaxies associated with SPT-CL J2040−4451 in the IRAC imaging data is also shown in Figure 2. All magnitudes are reported in the Vega system.

2.3. Optical Spectroscopy

Spectroscopic observations for SPT-CL J2040−4451 were carried out on the 6.5 m Baade Magellan Telescope on UT 2012 September 15 and 16 using the $f/2$ camera on the IMACS spectrograph with the 300-line grism at a tilt angle of 26°. The $f/2$ camera allows for slits to placed in a circular region with a diameter of $\sim 27'$. First night observations used the WBP 5694–9819 filter. After measuring a preliminary redshift of $z = 1.48$—somewhat higher than the photometric redshift, $z_p =$

Table 1
Imaging Observations of SPT-CL J2040−4451

UT Date	Telescope/Instrument	Filters	Exp. Time (s)	Depth[a]
2010 Oct 29	CTIO 4 m/MOSAIC-II	g, r, i	750,1200,1347	23.5,22.6,21.6
2011 Jul 14	CTIO 4 m/NEWFIRM	K_s	960	16.4
2011 Nov 3	CTIO 4 m/MOSAIC-II	z	2400	21.2
Cycle 7	*Spitzer*/IRAC	3.6 μm, 4.5 μm	800,180	20.3,18.8
2012 Jun 10,11	Magellan-I/FourStar	J	960	20.6
2012 Oct 4	Magellan-II/MegaCam	i'	1800	23.8

Note. [a] 10σ point source depths (Vega).

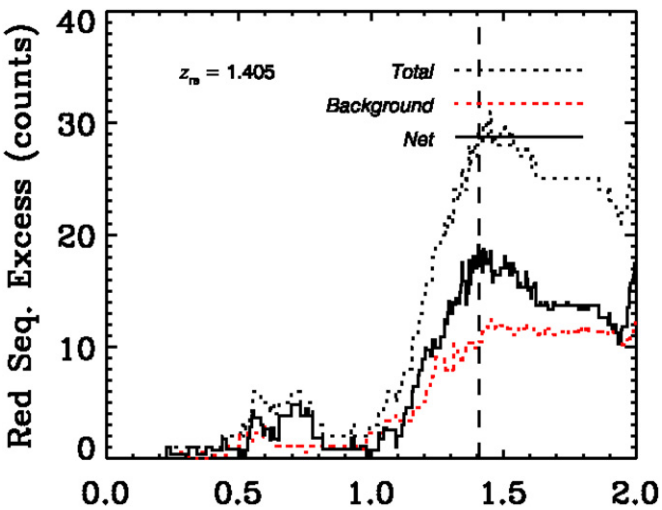

Figure 2. Photometric cluster confirmation, as applied to the SPT cluster sample described in previous SPT cluster papers (e.g., Song et al. 2012; Stalder et al. 2013). The excess number counts of candidate cluster members within a 2′ radius of the SPT coordinates for SPT-CL J2040−4451, based on *Spitzer*/IRAC 3.6–4.5 colors that are plotted (solid line), along with the total counts (dotted black line) and background counts (dotted red line) for comparison. Candidate cluster members here are identified as those being consistent within ±0.2 mag of the relation expected for a Bruzual & Charlot (2003) passively evolving galaxy population that formed at $z = 3$. There is a significant excess of galaxies indicating a cluster at $z_p = 1.405$.

(A color version of this figure is available in the online journal.)

1.41 ± 0.07—for numerous galaxies in the first night's data we modified the setup to include no spectroscopic filter in order to be more sensitive to Ca H and K redward of ∼9800 Å. The gain in sensitivity due to this change was negligible, as the throughput of the IMACS detectors drop of sharply redward of 9800 Å. Spectra of individual galaxies cover a typical wavelength range, $\lambda = 5700$–9820 Å.

The galaxy target selection for mask design was based on the optical and IR photometry presented in Song et al. (2012). That analysis identifies 62 candidate cluster member galaxies in *Spitzer* IRAC [3.6]−[4.5] versus [3.6] color–magnitude space. There is a strong sequence that forms for galaxies at a common redshift in this color–magnitude space (e.g., Brodwin et al. 2006; Muzzin et al. 2013), and we use it as our primary selection for likely cluster member galaxies. We refined the prioritization by using our available optical data to give highest priority to [3.6]−[4.5] versus [3.6] cluster candidates with faint counterparts in the z band, and we reject candidates with bright counterparts in multiple optical bands (e.g., $i' < 21$); likely low-redshift interlopers. Two multi-slit masks were designed with 1″.2 wide slits; this slit width choice throws away less light from our faint target galaxies, and the loss of spectral resolution does not significantly impact our ability to measure redshifts. The first mask was observed for a total integration time of 5.7 hr on UT September 15, and the second mask for 5.6 hr on UT September 16. Both nights were photometric with seeing between ∼0″.6–0″.9, and using the trace of a point source that fell within one of our slits we measure a spatial FWHM (along the slit axis) of 0″.85 in our final stacked two-dimensional (2D) spectra.

We use the COSMOS reduction package[37] to bias subtract, flat-field, wavelength calibrate and sky-subtract the raw data, resulting in wavelength-calibrated 2D spectra. The one-dimensional (1D) spectra are then boxcar extracted from individual source traces in the reduced data. The spectra are flux calibrated from observations of spectrophotometric standard LTT 1788 (Hamuy et al. 1994) taken during the run. Time series of the integrated flux measured for guide stars and DIMM stars throughout the nights of the run indicate that the nights were both photometric, with no evidence for significant changes in the atmospheric extinction across the two nights of the observing run. We find that the uncertainty in the flux calibration is dominated by variable slit losses over the course of the night that result from fluctuations in the seeing on timescales of minutes. We measure the scatter in the flux normalization directly from our data by measuring the variation in flux measured for well-detected objects in our masks across the individual exposures throughout the entire observing run. We find a scatter of ±20%, which results primarily from variations in slit losses over the course of the observations, consistent with slit loss variations from changes in the seeing and small variations in the exact alignment of the slit masks on the sky.

Spectral features are identified by eye in the 2D and 1D spectra, and cluster member redshifts are measured using the centroid of the blended [O II] line emission (we generally do not resolve the individual lines). The FWHM spectral resolution of the observations, as measured from sky lines that were extracted and stacked into 1D spectra in the same way as the science spectra, is 9.3 Å. From simulations using the noise properties of our reduced data we find that the final extracted spectra are sensitive to emission line fluxes $>3.8 \times 10^{-18}$ erg cm^{-2} s^{-1} within a spectral resolution element in the wavelength region $\lambda \sim 9000$–9400 Å, which corresponds to the location of [O II] λλ3727 at the cluster redshift.

3. RESULTS

3.1. Cluster Member Galaxies

SPT-CL J2040−4451 was initially measured to have a photometric redshift of $z = 1.37 \pm 0.07$ by fitting a model of passively evolved galaxies from Bruzual & Charlot (2003) to the available optical+NIR data; this process is described extensively in

[37] http://code.obs.carnegiescience.edu/cosmos

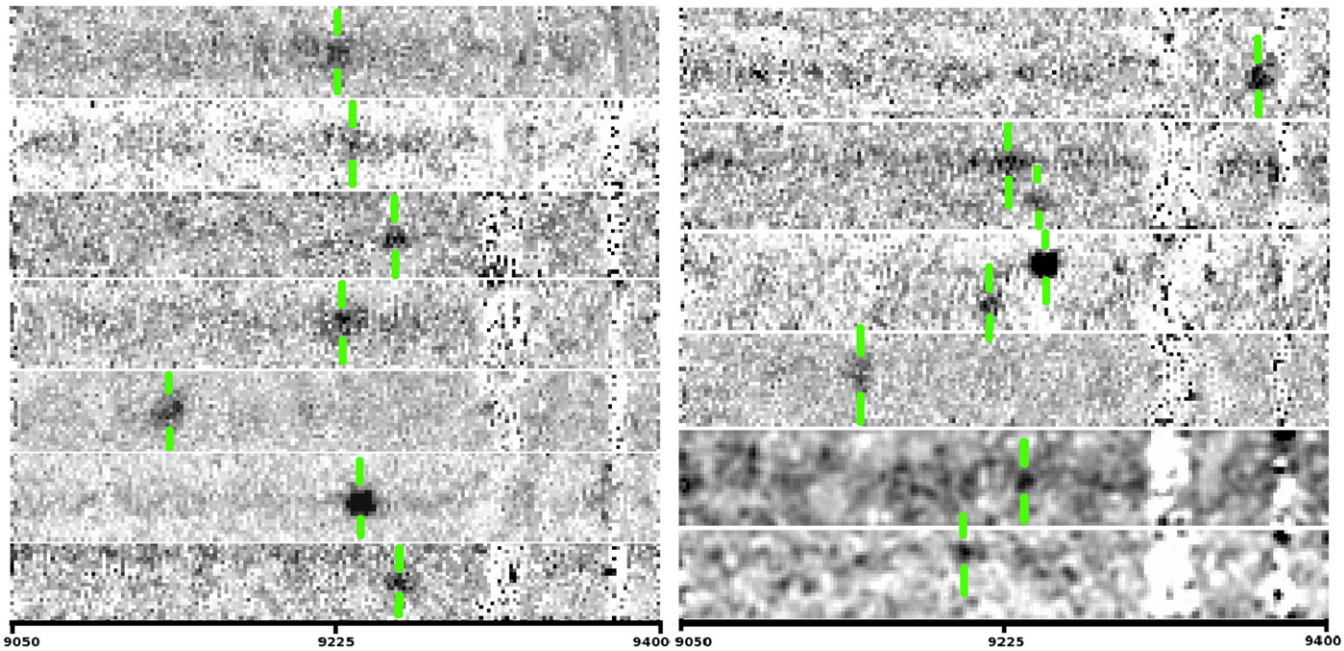

Figure 3. 2D sky-subtracted IMACS spectra containing the 15 [O II] emitting cluster member galaxies, with vertical green brackets indicate the [O II] emission. Each individual 2D spectrum spans the wavelength range, 9050–9400 Å. The two cutouts in the lower right have each been smoothed with a 2 pixel boxcar kernel to highlight the lower signal-to-noise detections in those spectra. Note that the 2D spectra data in the second and third cutouts from the top on the right side contain the two pairs of galaxies discussed in Section 3.4.

(A color version of this figure is available in the online journal.)

Table 2
Cluster Member Galaxies for SPT-CL J2040−4451

ID	R.A. (J2000)	Decl. (J2000)	z[a]	δz[a]	Megacam i'	$\delta i'$	IRAC [3.6]	δ [3.6]	IRAC [4.5]	δ [4.5]
J204110.1−444933.6	20:41:10.10	−44:49:33.6	1.4760	0.0006	23.16	0.07	16.95	0.03	16.35	0.03
J204100.1−445025.2	20:41:00.14	−44:50:25.2	1.4777	0.0006	24.11	0.17	17.28	0.03	16.82	0.03
J204057.0−445213.7	20:40:56.97	−44:52:13.7	1.4842	0.0006	24.91	0.26	20.58	0.40	20.80	0.40
J204100.9−445315.7	20:41:00.92	−44:53:15.7	1.4765	0.0006	23.17	0.12	17.43	0.03	16.88	0.03
J204057.2−445121.4	20:40:57.20	−44:51:21.4	1.4540	0.0006	24.01	0.15	19.43	0.04	19.91	0.20
J204057.3−445108.6	20:40:57.27	−44:51:08.6	1.4693	0.0009	23.42	0.08	18.97	0.33	18.99	0.17
J204113.6−445125.2	20:41:13.60	−44:51:25.2	1.4509	0.0005	23.97	0.13	18.92	0.04	18.69	0.15
J204058.1−445206.7	20:40:58.14	−44:52:06.7	1.4789	0.0005	22.86	0.07	18.48	0.03	18.22	0.04
J204054.6−445201.1[b]	20:40:54.61	−44:52:01.1	1.4842	0.0006	23.65	0.10	18.09	0.07	17.69	0.11
J204051.2−445116.8	20:40:51.15	−44:51:16.8	1.5120	0.0006	22.96	0.08	17.86	0.03	16.99	0.03
J204050.3−445020.5[b]	20:40:50.27	−44:50:20.5	1.4800	0.0006	24.60	0.21	18.98	0.25	19.20	0.40
J204048.5−445021.4	20:40:48.52	−44:50:21.4	1.4727	0.0006	22.06	0.06	18.09	0.03	17.49	0.03
J204044.2−445124.0	20:40:44.24	−44:51:24.0	1.4782	0.0006	22.91	0.07	17.34	0.03	16.77	0.03
J204050.4−445022.2	20:40:50.42	−44:50:22.2	1.4758	0.0006	23.01	0.08	17.22	0.03	16.69	0.03
J204048.7−445020.7	20:40:48.73	−44:50:20.7	1.4808	0.0006	23.32	0.08	19.15	0.14	18.84	0.10

Notes.
[a] Spectroscopic redshifts are measured from the blended [O II] doublet line emission, and uncertainties are dominated by the uncertainty in the centroid of a profile fit to the emission.
[b] These objects are adjacent to and blended with other bright sources in the IRAC imaging. We mask/subtract the contaminating light from these sources to measure the IRAC fluxes reported here, and assign them large errors reflecting the systematic uncertainty in the masking/subtraction.

Song et al. (2012). Incorporating additional follow-up data—specifically the Fourstar J band and Megacam i' band—refines the photometric redshift measurement to $z_p = 1.40 \pm 0.06$. At this redshift, we expected our IMACS observations to be sensitive to numerous spectroscopic features in cluster member spectra, including [O II] λλ3727, Ca II H and K, and the 4000 Å break. The IMACS spectra resulted in 15 galaxies with clear emission lines visible in the reduced 2D spectra in the wavelength range 9140 Å $< \lambda_{\rm obs} <$ 9370 Å (Figure 3), and no other emission lines elsewhere along the entire spectral trace extending to the blue limit of the spectra (∼5800 Å). Spectroscopic and photometric measurements of these likely cluster member galaxies are summarized in Table 2.

These emission lines are consistent with [O II] λλ3727 redshifted to $z \sim 1.48$. Furthermore, those lines with large signal-to-noise ratio (S/N) have line widths that are broader than the spectral resolution of the observations, consistent with the blended profile of the redshifted [O II] λλ3727 doublet (e.g., Figure 4). The lack of additional emission features blueward of the detected lines supports the hypothesis that these features

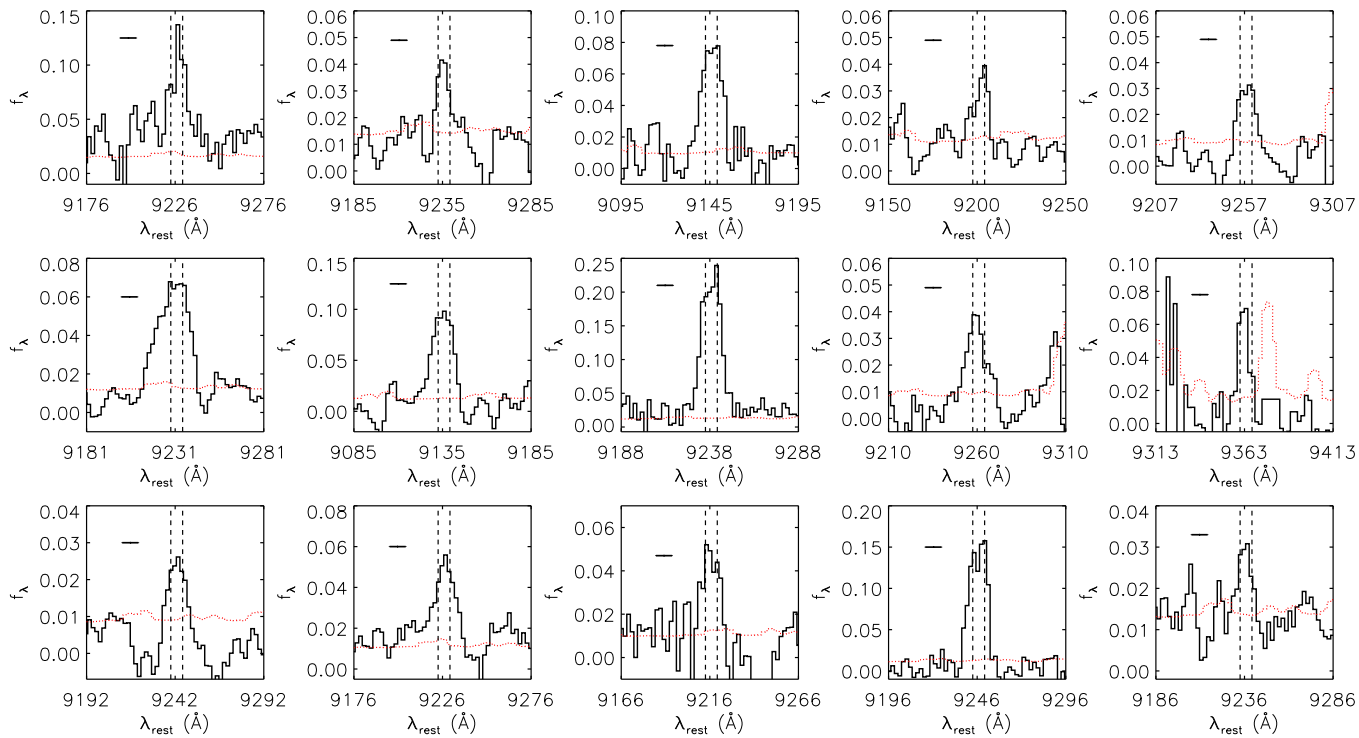

Figure 4. Individual 1D spectra of the 15 cluster member galaxies listed in Table 2 spanning an observed wavelength range of ±50Å on either side of the emission features shown in Figure 3. The *y*-axis values in each plotted spectrum are in units of erg s^{-1} cm^{-2} Å^{-1}, and the error array for each 1D spectrum in the same units is over-plotted as a red dotted line. Vertical dashed lines indicate the locations of the redshifted [O II] λλ3727,3729 emission features. Most of the emission features are broad or double-peaked, matching the expected [O II] doublet emission profile at our spectral resolution (indicated by the horizontal bar in each panel). Those lines that are not obviously broad are detected at very low signal-to-noise ratio (S/N) where the morphology of the line is not likely to be well measured at all.

(A color version of this figure is available in the online journal.)

Table 3
Outflowing Mg II Absorption in Star-forming Cluster Members

Galaxy ID	Mg II Redshift	Velocity Relative to [O II] (km s^{-1})
J204110.1−444933.6	1.4718	−510 ± 160
J204100.1−445025.2	1.4758	−230 ± 80
J204100.9−445315.7	1.4764	−250 ± 70
J204058.1−445206.7	1.4768	−20 ± 60
J204051.2−445116.8	1.5097	−280 ± 60
J204050.3−445020.5	1.4720	−970 ± 80

correspond to [O II] λλ3727, as the spectral coverage would include other bright nebular emission lines if the features that we observe were actually H–α, H–β, or O[III] λλ4960, 5008. Furthermore, six of the brightest [O II] emitting galaxies also have weak continuum absorption features that match the Mg II λλ2796, 2803 doublet at the same approximate redshift as the [O II] emission features (Figure 5)—these absorption features are blue-shifted with velocities ranging from −20 to −970 km s^{-1} relative to the emission lines in the corresponding spectra (Table 3), as would be expected for Mg II absorption lines from outflowing gas.

Five of the six outflow signatures have $v_{\rm outflow} \lesssim 500$ km s^{-1}, as is typical of outflows in the interstellar medium (ISM) due to winds in star-forming galaxies (Shapley et al. 2003), and one has a velocity, $v_{\rm outflow} = 970$ km s^{-1}, similar to those observed in the most vigorously star-forming galaxies (Weiner et al. 2009). These Mg II features are similar to those seen by, e.g., Papovich et al. (2010) in a galaxy cluster at $z = 1.62$. We note that one of the brighter line-emitting galaxies cannot be tested for the presence of Mg II absorption at $z \sim 1.48$ because the relevant part of the spectrum falls into an IMACS chip gap (the IMACS $f/2$ configuration uses fixed grism dispersers that cannot be adjusted to dither spectra along the dispersion direction). Another one of the brighter candidate cluster members exhibits possible Mg II absorption features that are unfortunately coincident in wavelength with the telluric *B* band, and is therefore excluded from Figure 5 and Table 3.

We also make a composite stack of all 15 spectra that we identify as cluster members. To stack we shift each spectrum into the rest frame based on the [O II] λλ3727,3729 emission feature, and mapping the shifted spectra to a common wavelength array (i.e., flux uniformly binned in wavelength) by linearly interpolating the shifted spectra. We then sum the flux from each of the member spectra, to produce the stack (Figure 6). We explored more complex stacking methods, such as median and averaging after applying a variety of sigma-clipping algorithms, but the resulting stack is qualitatively insensitive to method (i.e., they all have the same ISM absorption features and lack of Ne V emission lines. In this stacked spectrum we identify absorption features that correspond to Fe II λλ2586,2800 and Mg II λλ2796,2803 at a mean outflow velocity of ∼120 km s^{-1}, consistent with the handful of individual outflow signatures described above. In the stacked spectrum we also note a distinct lack of emission corresponding to the high-ionization [Ne V] λλ3346,3427, which argues against active galactic nucleus (AGN) activity as a dominant source of the observed [O II] emission. It is also apparent from Figure 6 that our data are not sufficiently sensitive in the rest-frame wavelength range containing the Ca II H and K absorption doublet to allow for a detection of those features. Based on all of the above evidence,

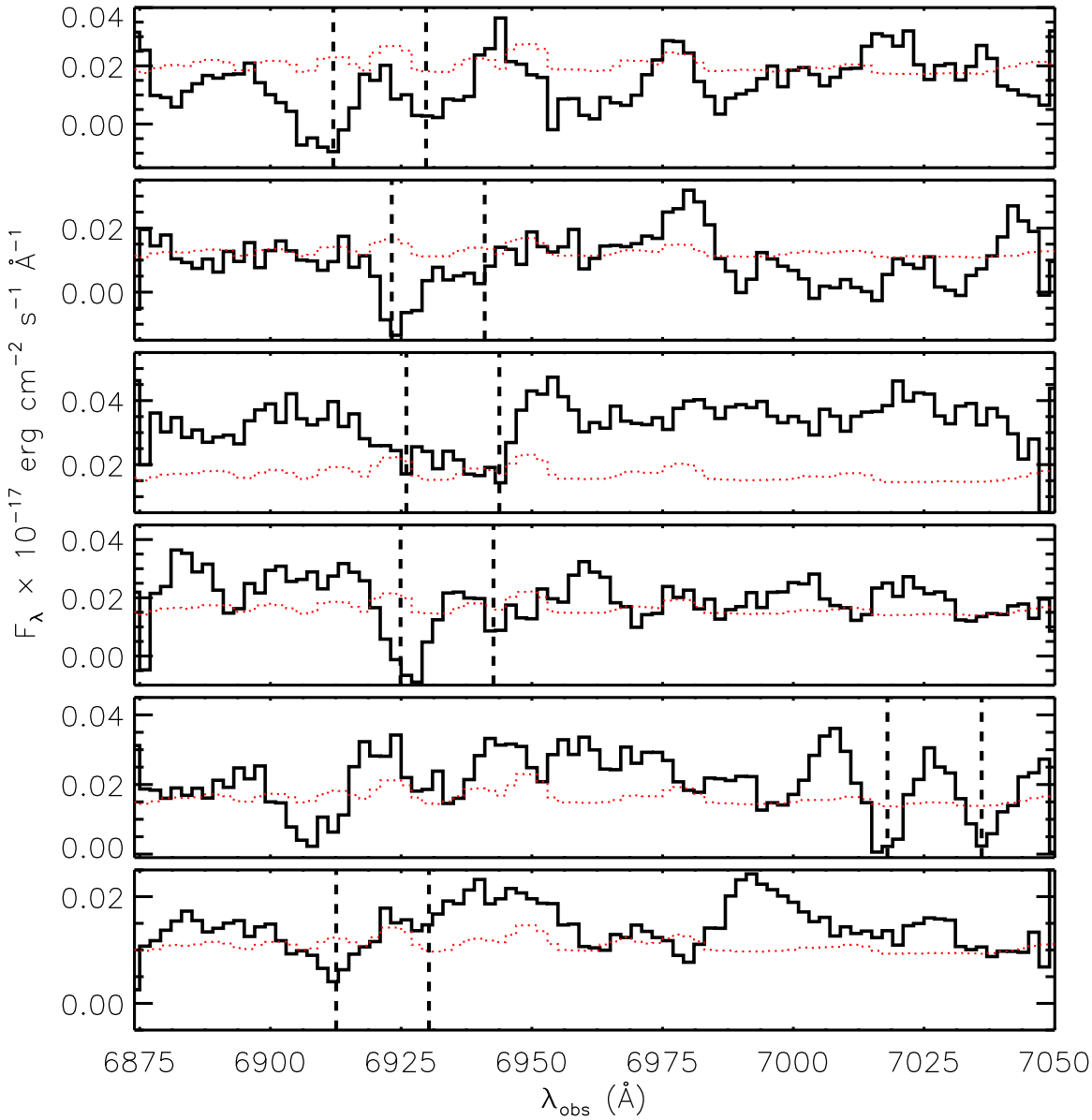

Figure 5. Extracted 1D spectra in the wavelength interval 6875 Å $< \lambda_{obs} <$ 7050 Å for the six spectroscopic cluster members that exhibit low S/N absorption features that are consistent with Mg II λλ2796,2803. The error array for each spectrum is plotted as a red dotted line. The spectra have been smoothed by a kernel matching the spectra resolution of the data. Vertical dashed lines indicate the locations of the apparent Mg II absorption lines. These absorption lines are not themselves especially robust, but taken in conjunction with the clear emission lines (Figure 3) confirm $z \simeq 1.48$ for the emission line galaxies.

(A color version of this figure is available in the online journal.)

we confidently conclude that the 15 observed emission lines are [O II] λλ3727 from member galaxies in SPT-CL J2040−4451.

At the spectroscopic redshift of the cluster the spectral features that are typically used to identify passive galaxies—primarily Ca H and K, and the 4000 Å break—are redshifted to wavelengths where the instrumental throughput of IMACS is falling rapidly toward zero and there are numerous bright sky lines (e.g., Figure 6). As a result we are unable to measure absorption line redshifts of passive cluster members in SPT-CL J2040−4451 with high confidence in the IMACS data. There are two red-sequence galaxies that could be considered the "brightest cluster galaxy" (BCG), with $m_{3.6\mu m} = 16.04$ and 16.16. Both of these galaxies are a factor of $\gtrsim$2 brighter than the next brightest galaxies at 3.6 μm, suggesting that they are substantially higher stellar mass. The presence of two nearly equally bright BCG candidates is reminiscent of the Coma cluster, which is in the late stages of a galaxy cluster merger (e.g., Colless & Dunn 1996; Biviano et al. 1996). Alternatively, we may simply be observing an epoch at which the dominant galaxy had yet to be established. For comparison, De Lucia & Blaizot (2007) simulate the hierarchical formation of BCGs and show that the dominant cluster galaxy may not be established until $z \lesssim 1.1$. Unfortunately we did not place a spectroscopic slit on the second brightest of these objects, and with the data presented in this work, we are unable to differentiate between these two scenarios.

We also note that the spectrum of one of the two potential BCGs—as described above—had a slit placed on it in the first of our two masks, and the resulting spectrum shows clear continuum emission redward of ∼8000 Å with no significant emission features, as would be expected for a passively evolving galaxy at $z \sim 1.48$. The spectrum is low S/N (∼2 per spectral pixel)

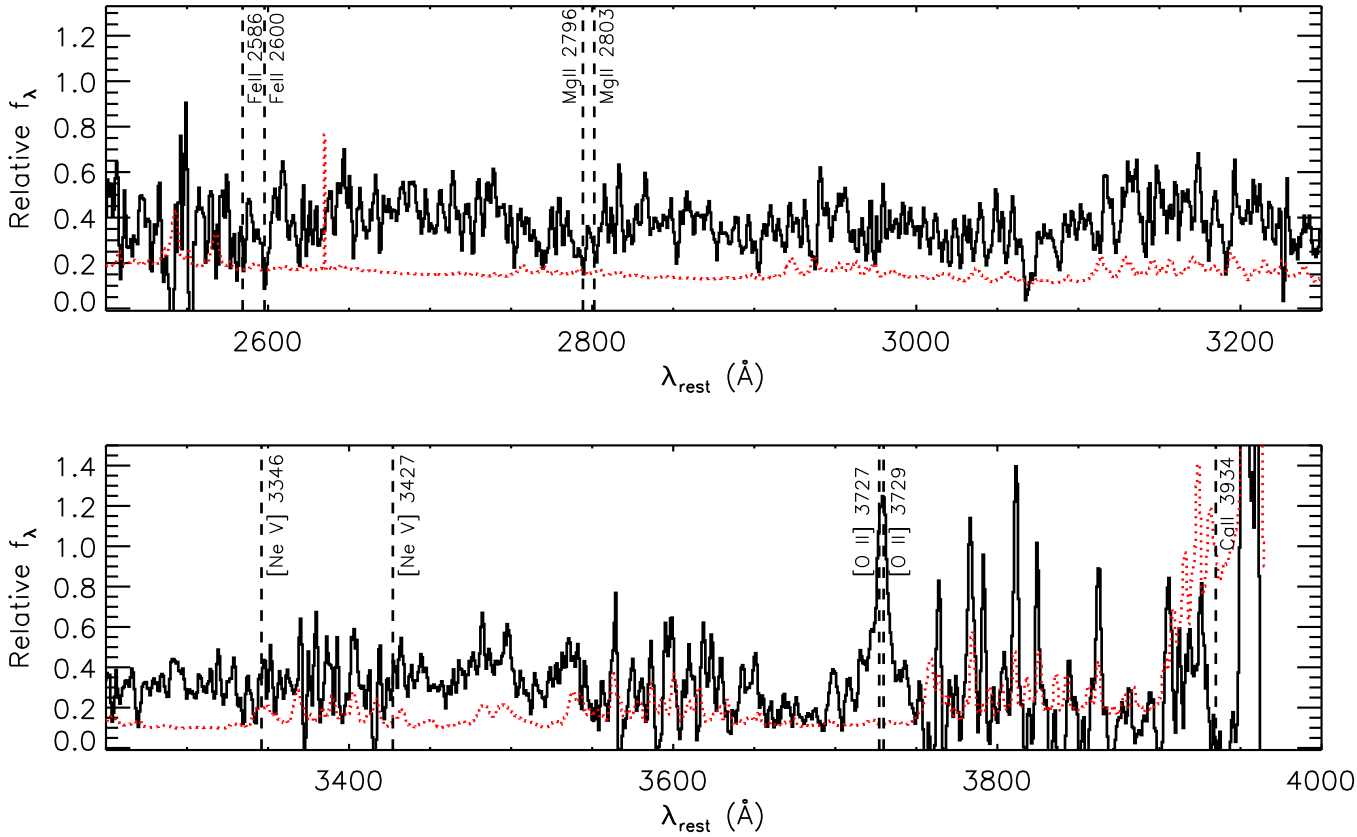

Figure 6. Stack of all 15 spectroscopic cluster member spectra, spanning the full wavelength range covered by the observations (∼6000–9800 Å, ∼2500–4000 Å in the rest frame). Top: the stacked spectrum in the rest-frame wavelength range $\lambda_{rest} = 2500$–3250 Å. The error array is over-plotted as the red dotted line. Vertical dashed lines indicate the presence of strong ISM absorption lines blue-shifted by ∼120 km s^{-1} relative to the [O II] λλ3727,3729 emission. Bottom: the stacked spectrum in the rest-frame wavelength range $\lambda_{rest} = 3250$–4000 Å, with the error array again over-plotted as the red dotted line. Vertical dashed lines here indicate the location of [O II] λλ3727,3729 emission, along with the predicted location of several un-detected features: two high-ionization [Ne V] forbidden lines (common in AGN) and the Ca II K absorption line.

(A color version of this figure is available in the online journal.)

and shows no strong features, which is typical of passive galaxy spectra in the rest-frame wavelength range ∼3200–3900—i.e., the rest-frame wavelengths sampled by our observations redward of 8000 Å at the cluster redshift. In addition to the potential BCGs, several other *Spitzer*-selected candidate cluster members have spectra that exhibit no signal (or S/N well below 1 per pixel) continuum redward of 8500–9000 Å, also consistent with potentially being passive galaxies at the cluster redshift. This consistency does, not, of course, preclude the possibility that some of these galaxies are late-type dwarf stars or other interlopers.

3.2. Star Formation in the Cluster

Our IMACS spectra provide [O II] λλ3727 flux measurements or lower limits for all 15 spectroscopically confirmed cluster member galaxies. We measure the flux by fitting a Gaussian to each emission line and integrating the total flux of the Gaussian fit. We allow for a local continuum level underneath each Gaussian fit and subtract the continuum off before integrating; in practice the continuum levels are consistent with zero and dwarfed by the emission line flux in all cases. The presence of [O II] λλ3727 emission is strong evidence of ongoing star formation, but converting from [O II] flux to SFR is an uncertain process (e.g., Yan et al. 2006; Lemaux et al. 2010). The observed [O II] line luminosity is very sensitive to dust extinction in the rest frame, but it is also possible for the observed [O II] emission to originate from an AGN rather than star formation. AGN emission should be spatially unresolved in our observations, as it would originate from a very small physical region in the cores of the galaxies, whereas line emission from star-forming regions should be distributed throughout the galaxies and result in extended emission. As previously noted, we do not find any [Ne V] emission the stacked spectrum of the 15 cluster members, which argues against the kind of hard ionizing spectrum that would result from strong AGN activity (Figure 6). We also find that the emission line profiles along the spatial axis (i.e., along the slit) are extended relative to a point source (Section 2.3) for all but one of the 15 spectroscopic cluster members, and this single exception (J204057.0−445213.7) is one of the lower S/N detections in our spectroscopic data, where the spatial FWHM measurement is significantly uncertain. From the above evidence we conclude that the [O II] that we observe is not likely to be AGN-dominated. We cannot rule out a low, subdominant level of AGN contribution to the measured [O II] fluxes for the member galaxies of SPT-CL J2040−4451. We do note that it is possible that some of the [O II] emission that we observe is associated with low ionization nuclear emission-line region (LINER) processes. LINER line emission is not directly associated with star formation and is sometimes observed to be spatially extended, but is also not necessarily associated with AGN activity in all cases (Yan & Blanton 2012). From our data we lack the information necessary to precisely identify LINER-like galaxies in our sample.

Table 4
Emission Line Properties of Confirmed Cluster Members

ID	$R_{\rm proj}$ (Mpc h_{70}^{-1})	$v_{\rm peculiar}$ (km s^{-1})	(O II)[a] ($\times 10^{-17}$) (erg cm^{-2} s^{-1})	SFR$_{\rm [OII]}$ ($M_\odot$ yr^{-1})
J204110.1−444933.6	1.454	−240 ± 40	3.99 ± 1.04	8.0 ± 3.2
J204100.1−445025.2	0.607	−30 ± 40	1.27 ± 0.61	2.6 ± 1.4
J204057.0−445213.7[b]	0.384	750 ± 40	>1.63 ± 0.51	>3.3 ± 1.4
J204100.9−445315.7	0.878	−180 ± 40	4.96 ± 1.22	10.0 ± 3.9
J204057.2−445121.4[b]	0.222	−2900 ± 40	>3.66 ± 0.90	>7.1 ± 2.7
J204057.3−445108.6[b]	0.292	−1050 ± 60	>0.81 ± 0.37	>1.6 ± 0.9
J204113.6−445125.2	1.306	−3270 ± 30	5.97 ± 1.36	11.5 ± 4.3
J204058.1−445206.7	0.283	110 ± 30	11.5 ± 2.36	23.1 ± 8.4
J204054.6−445201.1[b]	0.472	760 ± 40	>1.90 ± 0.58	>3.9 ± 1.7
J204051.2−445116.8	0.750	4100 ± 40	1.73 ± 0.59	3.7 ± 1.7
J204050.3−445020.5[b]	1.036	250 ± 40	>0.82 ± 0.41	>1.7 ± 1.0
J204048.5−445021.4[c]	1.162	640 ± 40	>1.47 ± 0.53	>2.9 ± 1.4
J204044.2−445124.0	1.364	30 ± 40	0.72 ± 0.47	1.5 ± 1.0
J204050.4−445022.2	1.015	−260 ± 40	2.22 ± 0.69	4.5 ± 1.9
J204048.7−445020.7[c]	1.148	340 ± 40	>7.90 ± 1.68	>16.0 ± 5.9

Notes.
[a] [O II] flux measured within $\pm 2\sigma$ of the line centroid, uncorrected for slit losses, which should be very small for objects that were the primarily targets of individual mask slits.
[b] These galaxies fell serendipitously onto slits, and therefore likely suffered significant slit losses that are difficult to quantify robustly, so we report the measured [O II] flux as a lower limit.
[c] These objects appear as a blend of two sources in the IRAC catalogs that were used to design our spectroscopic masks, such that the mask slit falls partially onto both sources. As a result we avoid attempting an ad hoc correction for slit losses and report the measured [O II] fluxes and SFRs as lower limits.

Given [O II] λλ3727 flux measurements, we can make a very rough attempt at estimate the SFR within each [O II] emitting galaxy. These estimates are, however, subject to serious caveats due to corrections that must be made to account for slit losses in our spectroscopy, as well as suppressed [O II] emission due to dust extinction. Rosa-González et al. (2002) provide an empirical prescription for SFR estimates based on rest-frame optical and UV observables that attempts to use correlations between SFR and dust properties to correct for underestimates of the SFR due to extinction. Using [O II] λλ3727 luminosity, this amounts to a factor of six times increase in the estimated SFRs relative to the Kennicutt (1998) Case B relation. This is the best estimate that we can use to correct for the dust extinction in our galaxies, due to the lack of a means to measure the dust extinction within our individual galaxies. Correcting for slit losses is a highly uncertain process for the spectra reported in this paper that correspond to the serendipitously detected galaxies (those galaxies that fell partially onto a slit that was centered on a different source). This is because the serendipitous sources are not centered on a slit, and therefore are subject to huge slit loss uncertainties as a function of variations in the seeing. For these galaxies we report only lower limits on the total line flux due to the extreme uncertainty in computing slit loss corrections; these limits correspond to lower limits in the inferred SFR from [O II] λλ3727.

Using a standard cosmology (see Section 1) we compute the corresponding luminosity in [O II] along with the corresponding SFR assuming Case B recombination and the Kennicutt (1998) relationships between nebular line emission and the rate of star formation. It would be ideal to have additional star formation indicators for SPT-CL J2040−4451, but the available data—including *WISE* photometry—are to shallow by more than an order of magnitude to make a measurement or place interesting limits. We also measure the projected distance between each cluster member and the cluster centroid as measured via the SZ effect; these impact parameters can be compared to the radius, R_{200}, at which the interior mean density of the cluster is 200 times the mean density of the universe at the cluster redshift, $\rho_m(z)$. The $M_{200,\rm SZ}$ value computed in Section 3.3 implies R_{200} for SPT-CL J2040−4451 of 1.2 Mpc. All 15 spectroscopically confirmed cluster members are within 2′.85—a projected distance of approximately 1.5 Mpc—of the centroid of the SZ signal as measured by the SPT. Individual projected distances, [O II] fluxes, and [O II]-based SFR estimates are presented in Table 4.

3.3. SZ Mass Estimate

We update the SZ mass estimate from Reichardt et al. (2013), incorporating the newly measured spectroscopic redshift for SPT-CL J2040−4451. The SZ mass is calculated using a Markov chain Monte Carlo (MCMC) method that fits the SZ mass–observable scaling relations while marginalizing over ΛCDM cosmological parameters, and incorporates constraints available from X-ray data for 14 SPT clusters, as well as observations of the CMB, the cosmic baryon density measured from primordial deuterium abundance, baryon acoustic oscillations, distance measurements from Type Ia supernovae, and the galaxy cluster mass function as measured by the SPT. The MCMC method is described in more detail in Reichardt et al. (2013) and Benson et al. (2013). The resulting mass is defined as the mass within a radius, r_{500}, within which the cluster has a mean matter density that is 500 times the critical density of the universe, $\rho_c(z)$, and is calculated to be $M_{500,\rm SZ} = 3.2 \pm 0.8 \times 10^{14}\, M_\odot\, h_{70}^{-1}$. This mass estimate includes measurement noise, noise due to astrophysical contaminants, and the systematic errors due to the uncertainties in scaling relation parameters and cosmological parameters. It is also common to report galaxy cluster masses within the radius r_{200}, which encloses a region that is 200 times the *mean* density of the universe; assuming

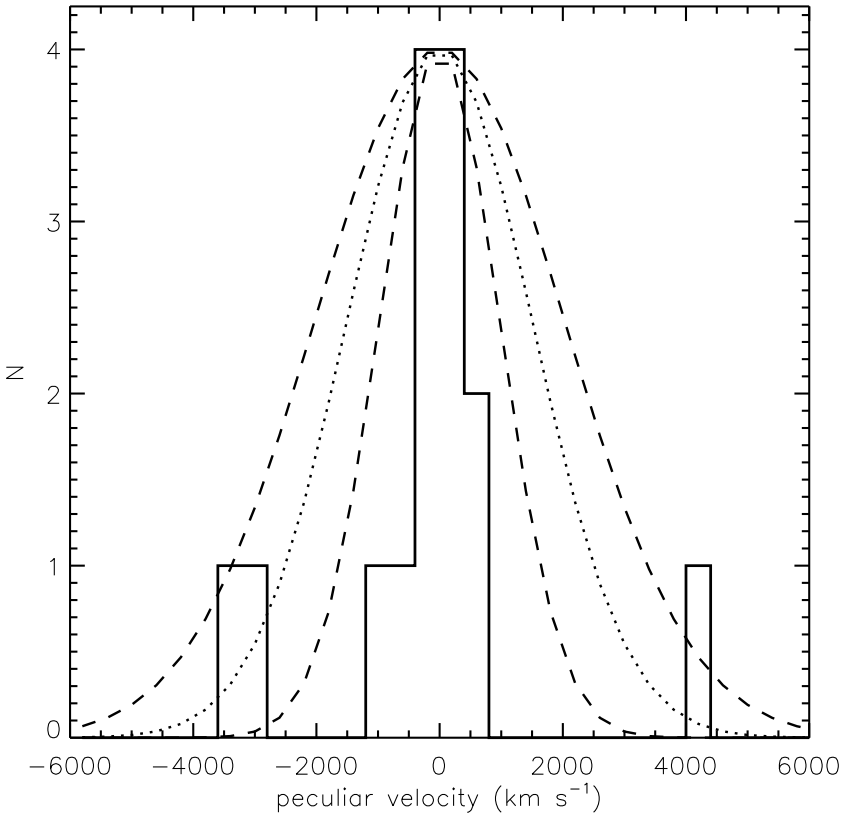

Figure 7. Rest-frame velocity histogram for SPT-CL J2040−4451, with peculiar velocities grouped into bins of 400 km s^{-1} and the estimate of the velocity dispersion over-plotted (dotted line), along with the velocity distributions corresponding to the jackknife 1σ uncertainties (dashed lines) in the dispersion.

the Navarro–Frenk–White profile shape (Navarro et al. 1997) for the cluster density profile and using a value for the concentration parameter taken from the mass–concentration relation as measured in simulations (Duffy et al. 2008), it becomes straightforward to convert between masses measured at different overdensity radii (Hu & Kravtsov 2003). The r_{200} SZ-based mass estimate for SPT-CL J2040−4451 is $M_{200,\mathrm{SZ}} = 5.8 \pm 1.4 \times 10^{14} M_{\odot}\, h_{70}^{-1}$.

The existence of massive galaxy clusters at relatively early epochs of the universe has the potential to test the viability of cosmological models, and with both a mass and redshift in-hand for SPT-CL J2040−4451 we can quantify its rarity (or lack thereof). Following the procedure in Section 4.1 of Stalder et al. (2013), we can estimate how many clusters at least as rare as SPT-CL J2040−4451 that we would expect in the SPT-SZ survey. Given the best-fit mass function and scaling relation from Reichardt et al. (2013), we expect approximately 0.7 clusters with simultaneously higher mass and redshift than SPT-CL J2040−4451. If we consider an ensemble of 720 deg^2 of SPT-SZ survey area (i.e., the sample in Song et al. 2012) then we find that we are very likely (>99%) to have found a cluster at least as rare as SPT-CL J2040−4451. Running the same test for the full 2500 deg^2 SPT-SZ survey area we naturally also find that it is very likely that we should (>99%) find a cluster at least as rare as SPT-CL J2040−4451.

3.4. Velocity Dispersion

Our ability to compute a reliable velocity dispersion is fundamentally hindered by the small number of available cluster member velocities. However, given the paucity of spectroscopically confirmed members in known high-redshift galaxy clusters, the spectroscopy presented here for SPT-CL J2040−4451 represents one of the best-sampled velocity distributions for a galaxy cluster at $z > 1.2$. It is therefore interesting to investigate the dynamics of SPT-CL J2040−4451, while keeping in mind the caveat that the sample used is limited to 15 spectroscopic galaxies.

We compute the velocity dispersion from the sample of 15 cluster members with emission line redshifts using the a gapper statistic similar to that described by Beers et al. (1990). The biweight estimator is commonly used in the literature to measure the dispersion in peculiar velocities of cluster members, but Beers et al. (1990) point out that the gapper statistic is more robust for sparsely sampled distributions (e.g., $N \leqslant 15$) so we use a gapper estimate in this work to produce the most reliable estimate. The velocity dispersion of SPT-CL J2040−4451 is $\sigma_{v,\mathrm{gap}} = 1500 \pm 520\,\mathrm{km\,s^{-1}}$, where the uncertainties are computed using the jackknife method. For reference, both the biweight and simple standard deviation estimates of the dispersion for SPT-CL J2040−4451 (1600 and 1660 km s^{-1}, respectively) are in reasonable agreement with the gapper value. The velocity distribution is shown in Figure 7, along with the estimated distribution and its jackknife uncertainties.

We note that of the 15 spectroscopic cluster members, there are two pairs of cluster members that are separated by small ($\lesssim 3''$; $\lesssim 30$ kpc h_{70}^{-1}) angular distances on the sky (second and third cutouts from the top on the right side of Figure 3). Each of these pairs corresponds a slit on our custom spectroscopic slit masks that yield spectral traces for two different galaxies at the cluster redshift. From the data we know that these galaxies are located close together in both projected distance on the sky, and in recession velocity. There are several possible physical interpretations of these pairs: (1) they could be two cluster member galaxies that appear as a chance projection

(i.e., galaxies within the cluster that are separated by a large distance in the radial direction), (2) they could be cluster member galaxies that are physically close to one another, or (3) each pair could in fact be [O II] emission from two star-forming regions within a single galaxy. In each case the pairs of galaxies are separated in velocity space by $dv > 500\,\mathrm{km\,s^{-1}}$, which allows us to rule out the possibility that each pair is really just two different star-forming regions within the same galaxy. Given the limited phase space information we cannot measure the true phase space coordinates of each galaxy pair, however, and therefore we cannot distinguish between the first and second possibilities above. If one or both of these galaxy pairs are, in fact, located physically close to one another then it is possible that they are parts of some subhalo/substructure within the larger cluster potential. If this is the case then these galaxies are not all necessarily providing independent samplings of the total cluster potential. There is possible evidence for this subhalo sampling in the velocity distribution, shown in Figure 7, where there is a concentration of cluster member velocities with a small dispersion and three more outlying galaxies. We also note that three of the 15 galaxies that we have identified as members have very large peculiar velocities ($\gtrsim 3000\,\mathrm{km\,s^{-1}}$) relative to the bi-weight median, and one or more of these could be interlopers in the velocity distribution, but are not rejected by 3σ cuts with the current 15 member velocity sample. Naturally, if we were to classify these three galaxies as interlopers then the resulting dispersion estimate would be smaller—still with very large uncertainties and consistent with the SZ-based mass estimate.

The dispersion estimated from the 15 members is poorly constrained, with a 2σ range of $\sim$500–2500 $\mathrm{km\,s^{-1}}$. If we apply the scaling relation between velocity dispersion and virial mass of Evrard et al. (2008) then this corresponds to a mass of $M_{200,\sigma} = 1.8^{+2.5}_{-1.3} \times 10^{15} M_\odot\, h_{70}^{-1}$, which is both extremely large and extremely uncertain. However, it is also physically unreasonable to expect the velocity dispersion estimated here to be related to the cluster mass in the same way as that of a dynamically relaxed population of galaxies (e.g., passive, early type). All 15 spectroscopically confirmed members of SPT-CL J2040−4451 exhibit strong [O II] emission, and numerous studies have empirically confirmed that the velocity dispersions measured from blue/late-type/star-forming galaxies in clusters—which tend to be infalling—are larger than the dispersion of their passive counterparts (Girardi et al. 1996; Mohr et al. 1996; Carlberg et al. 1997; Koranyi & Geller 2000; Goto 2005; Pimbblet et al. 2006). Studies using simulations similarly find that cluster velocity dispersions measured using blue galaxies are larger than those measured from red galaxies (Gifford et al. 2013).

It is, therefore, interesting to proceed with the hypothesis that our sample of spectroscopic cluster members are all infalling, and may be treated as test particles falling into the cluster potential. In this scenario, their line of sight velocities distribution would reflect the free fall velocity, rather than the velocity dispersion, associated with the cluster mass. As mentioned above, it has been shown in observations and simulations that cluster velocity dispersions computed using blue galaxies are, on average, systematically larger than those computed from red/passive galaxies, which qualitatively affirms a physical scenario in which the distribution of blue galaxy velocities trace the cluster potential via infalling rather than virialization. The equation relating the free fall velocity, v_{ff}, to the attracting mass, assuming the galaxies began falling from some distance, $r \gg R$, is $M(<R) \simeq (R v_{\mathrm{ff}}^2/2G)$, where R is the current distance between an infalling galaxy and the center of mass of the cluster. We can use the projected distance of the galaxies from the cluster center (Table 4)—assuming that their trajectories are randomly oriented on the sky—to estimate the median distance from the 15 member galaxies to the center of SPT-CL J2040−4451. The median projected distance on the sky, $\bar{R}_{\mathrm{proj}}$, of the 15 member galaxies is 0.88 Mpc (corresponding to $\bar{R} = 1.8$ Mpc after de-projection assuming velocity vectors randomly oriented on the sky), and solving for the mass here gives $M(<\bar{R}) \simeq 5 \times 10^{14}\, M_\odot\, h_{70}^{-1}$, consistent with the mass estimated from the SZ signal. We do not advocate for this method as a way to precisely estimate cluster masses, but we do note that the results of this free-fall picture are consistent with the SZ mass estimate, and makes sense in the context of a physical picture in which the 15 [O II] emitting galaxies are predominantly infalling cluster member galaxies.

4. DISCUSSION

4.1. Cluster Members In Color–Magnitude Space

In Figure 8 we plot the results of our spectroscopy on top of the optical+NIR $i'-[3.6]$ versus [3.6] and IRAC NIR only [3.6]−[4.5] versus [3.6] color–magnitude diagrams (CMDs) for SPT-CL J2040−4451. The IRAC-only CMD is useful for identifying an over-density of galaxies in redshift based on the presence of the rest-frame 1.6 μm "stellar bump" feature that is ubiquitous in older stellar populations with similar ages and formation histories (e.g., Brodwin et al. 2006; Muzzin et al. 2013), while the optical+IRAC CMD is sensitive to red/passively evolving galaxies at a common redshift. Object prioritization for spectroscopic mask design was based primarily on the *Spitzer* CMD, and it is clear that the objects that form a tight sequence in [3.6]−[4.5] versus [3.6] are not tightly clustered in $i'-[3.6]$ versus [3.6] space—i.e., they are not a monolithic passively evolving population of galaxies. The spectroscopically identified star-forming cluster members tend to occupy the "blue cloud" region in the $i'-[3.6]$ versus [3.6] CMD, as expected.

In addition to the population of actively star-forming galaxies revealed in our spectroscopy, there is also evidence for a possible significant population of passive cluster members. Their presence can be inferred from the extremely low S/N continuum emission that we observe in MOS slits placed on photometrically selected cluster member galaxies. There are 20 such objects plotted as red X's in Figure 8, though only 10/20 have i'-band detections. Those without cannot be included in the $i'-[3.6]$ versus [3.6] CMD. We cannot claim that these 20 galaxies are all passive cluster members, but it is unlikely that most or all of them are interloping passive galaxies given that they have IRAC colors that are consistent with a population of galaxies at the spectroscopic redshift of SPT-CL J2040−4451. It is also encouraging that half of these putative passive member galaxies with i'-band detections fall within 0.2 mag of the red sequence predicted for a population of passively evolving galaxies at the cluster redshift. Deeper spectroscopic observations, preferably using the nod-and-shuffle technique in the optical, or one of the new generation of multi-object NIR spectrographs, will be necessary to unambiguously identify passive member galaxies of SPT-CL J2040−4451.

The ground-based NIR imaging that is currently available for SPT-CL J2040−4451 is not sufficiently deep to allow us to

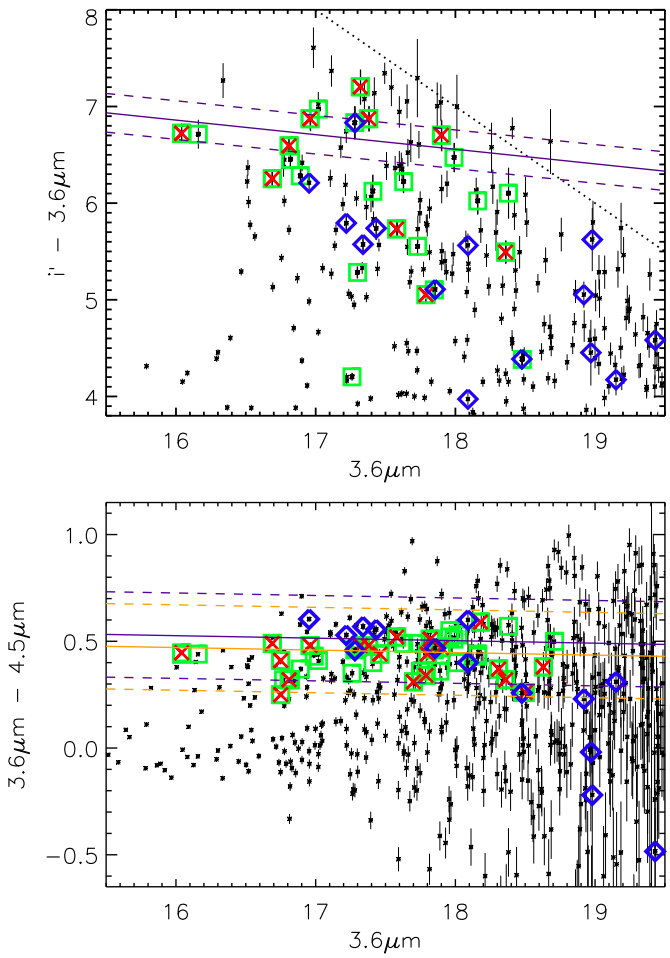

Figure 8. Color–magnitude diagrams for SPT-CL J2040−4451 using the best available optical and NIR photometry—Megacam i' band, plus [3.6] and [4.5] from *Spitzer*+IRAC. All sources that have detections in the IRAC and Megacam imaging (i.e., essentially everything within an area on the sky set by the IRAC field of view) are plotted as small black asterisks, with candidate cluster members identified from the *Spitzer* photometry over-plotted as green squares. *Spitzer*-selected cluster candidates that were targeted by spectroscopic slits in our 2012 September IMACS MOS observations but did not yield a redshift are also identified by red X's, and cluster members confirmed via [O II] emission are marked with blue diamonds. Galaxies plotted as empty green squares were photometrically identified cluster members that did not receive a slit in the mask design process. Top: $i'-$ [3.6] vs. [3.6]. The diagonal dotted line indicates the color–magnitude selection corresponding to the 50% completeness limit in our i'-band photometry. Over-plotted in purple is the red sequence from Bruzual & Charlot (2003) models with a Chabrier initial mass function (Chabrier 2003) and solar metallicity, assuming a single burst of star formation at $z = 5$. Bottom: [3.6]−[4.5] vs. [3.6] with Bruzual & Charlot (2003) models—±0.2 mag in color—at $z = 1.41$ (photometric cluster redshift; orange) and $z = 1.478$ (purple).

(A color version of this figure is available in the online journal.)

construct a CMD which narrowly brackets the 4000 Å break in order to isolate passive cluster members e.g., $i'-J$ versus J or $i'-K_s$ versus K_s. Deeper NIR imaging in the ∼1–2.3 μm range would allow us to identify the red sequence, and facilitate a measurement of the LF of the passive galaxy population.

4.2. Prevalence of Star-forming Cluster Members

The abundance of strong [O II] emitting galaxies in SPT-CL J2040−4451 stands in stark contrast to other spectroscopically confirmed $z > 1$ SPT clusters, and is consistent with the model discussed above, likely reflecting both its lower mass and higher redshift relative to the majority of the SPT cluster sample, which are mass selected to satisfy $M_{500,\mathrm{SZ}} > 3 \times 10^{14}\ h_{70}^{-1} M_\odot$, and have a median redshift of $z = 0.55$. Given the incompleteness of our spectroscopic coverage (i.e., we do not have spectroscopy of a magnitude limited sample), it is difficult to quantify the abundance of star-forming members in an absolute sense. However, what we *can* do is compare the abundance of star-forming members in SPT-CL J2040−4451 relative to other high-redshift cluster that were observed with the same spectroscopic strategy (slit placement and object prioritization) as the data presented in this paper.

The IMACS observations presented here included a total of 59 slits, resulting in 15 [O II] emitters (i.e., a "hit rate" of 25.4% ± 7%). These IMACS observations result from masks designed using the same data as an input—primarily *Spitzer*/IRAC photometry—and using the same object selection criteria as SPT-CL J0546–5345, SPT−CL J2106-5844, and SPT-CL J0205−5829, at z =1.067, 1.132, and 1.320, respectively (Brodwin et al. 2010; Foley et al. 2011; Stalder et al. 2013). The IRAC photometry is sensitive to galaxies deep down the LF at all of these redshifts (M^* + 2.5 at $z \sim 1.5$), such that IRAC color-based selections are not biased, e.g., picking out only the brightest cluster members at higher redshifts. Additionally, all of these high-z SPT clusters were observed with equivalent wavelength coverage and spectral resolution, similar integration times, and in similar conditions. Observations of each of these three previously published systems resulted in ⩽3 emission line cluster member galaxies per cluster, and we can compute the hit rate for [O II] emitting cluster members resulting from spectroscopic slits. The resulting hit rates are 4% ± 3%, 2% ± 2%, and 2% ± 2% for SPT-CL J0546−5345, SPT-CL J2106−5844, and SPT-CL J0205−5829, respectively. Additionally, the emission line cluster members in these three previously published SPT-discovered clusters exhibit less observed [O II] flux than the star-forming galaxies in SPT-CL J2040−4451.

The identification here of 15 strong emission line galaxies implies that SPT-CL J2040−4451 is experiencing a period of star formation that far exceeds the other spectroscopically studied SPT galaxy clusters at $z > 1$. The discovery of SPT-CL J2040−4451 at $z = 1.478$ marks the first SZ-detected galaxy cluster to be observed in an epoch in which even moderately massive clusters (e.g., $\sim 5 \times 10^{14}\ M_\odot$) have not yet settled into the mode of passive evolution that is associated with massive, evolved clusters at lower redshift.

As indicated in Figure 8 and discussed in Section 3.1, there is also some evidence for a population of passive members in SPT-CL J2040−4451, for which our instrument and spectroscopic setup were not well suited to measure redshifts. Further multi-wavelength observations of SPT-CL J2040−4451 will be necessary to fully characterize the passive and star-forming galaxy populations, but the significant abundance of strong [O II] emitting galaxies revealed by our spectroscopy is a strong indication that this galaxy cluster is undergoing significant build-up of new stellar mass, similar to other high-redshift clusters discovered at other wavelengths.

Detailed studies of other high-redshift clusters find evidence for assembly of cluster member galaxies through increased merging activity. For example, in *Hubble Space Telescope* imaging of ClG J0218.3−0510 at $z = 1.62$, Lotz et al. (2013) observe a high incidence of double-nuclei galaxies and close galaxy pairs in candidate cluster member galaxies with large stellar mass ($\gtrsim 3 \times 10^{10}\ M_\odot$), from which they infer a merger rate as much as an order of magnitude higher than in similarly

massive field galaxies at the same redshift. Tran et al. (2010) also measure a high star formation density ($\sim$1700 $M_{\rm sun}$ yr^{-1} Mpc^{-1}) in ClG J0218.3−0510 at $z = 1.62$ using a combination of 10-band spectral energy distribution fitting and spectroscopy. Rudnick et al. (2012) use the measured LF of red sequence members in ClG J0218.3−0510 to argue that increased mergers are necessary to describe the build-up of galaxies in clusters. Zeimann et al. (2012) also find high SFRs traced by rest-frame nebular emission lines in spectroscopically confirmed members of IDCS J1433.2+3306—an optical+NIR selected cluster at $z = 1.89$.

Looking beyond individual high-z clusters, several groups have also measured the properties of cluster member galaxies in larger samples of high-redshift galaxy clusters. *Spitzer*/IRAC imaging can be used to identify color-selected cluster member galaxies based on the 1.6 μm bump feature, which can identify galaxies that are passive, or actively star forming, or in the processes of transition from one the other. Mancone et al. (2010) measure *Spitzer*/IRAC [3.6] and [4.5] LFs for binned samples of optical+NIR selected galaxy clusters, and find disagreement between the measured LF in $z \gtrsim 1.3$ clusters and the assumed passive evolution model, which they suggest could be evidence for ongoing galaxy mass assembly. Similarly, in a sample of 16 *Spitzer*-selected clusters, Brodwin et al. (2013) combine *Spitzer* MIPS, IRAC, optical, and spectroscopic data to characterize the formation histories of cluster member galaxies; they show evidence for a systematic increase in star formation at $z \gtrsim 1.4$, and propose a model in which galaxy clusters undergo an epoch of frequent merging activity that resembles group environments in the local universe (Hopkins et al. 2008). In this model, merger activity falls off steeply as clusters become more relaxed, with larger internal velocity dispersions.

5. SUMMARY AND CONCLUSIONS

We present the discovery and follow-up observations of SPT-CL J2040−4451, with a spectroscopic redshift of $z = 1.478$. It is the highest-redshift, spectroscopically confirmed, SZ-discovered cluster known. We combine the newly measured redshift with SPT observations to infer a mass of $M_{500,\rm SZ}$ (M_{200}) $= 3.2 \pm 0.8$ (5.8 ± 1.4) $\times 10^{14}\, M_\odot h_{70}^{-1}$, making SPT-CL J2040−4451 one of the most massive clusters known at $z > 1.4$. We estimate the cosmological rarity of SPT-CL J2040−4451, and find that it is not surprising to find a cluster of this mass and redshift in the SPT-SZ survey.

From our optical spectroscopy we identify 15 cluster members with [O II] $\lambda\lambda$3727 emission, all of which exhibit SFRs $\geqslant$1.5 $M_\odot$ yr^{-1}. The abundance of star-forming galaxies observed in SPT-CL J2040−4451 relative to other high-z SPT-detected clusters agrees well with recent observations that reveal elevated star formation in galaxy clusters at $z \gtrsim 1.4$. We measure a velocity dispersion of the star-forming cluster members of $\sigma_v = 1500 \pm 520$ km s^{-1}. However, we argue that this measurement is likely biased high, relative to the expectation from the dark matter halo mass, due to the fact that all of the measured cluster members are star forming, and therefore more likely to be drawn from the population of galaxies that are infalling into the cluster, rather than the dynamically relaxed population of passive cluster member galaxies.

Notably, SPT-CL J2040−4451 is not only the highest-redshift cluster in the current SPT catalog, but it is also near the low end of the mass range that the SPT-SZ survey samples. Studying the epoch of star formation in the progenitors of the most massive galaxy clusters requires that we investigate cluster assembly as a function of both redshift *and* mass. It is therefore important to use samples of high-redshift clusters that can be precisely classified as a function of mass. A significant advance toward this goal has been achieved with the recently completed 2500 deg^2 SPT-SZ survey, which provides a nearly mass-independent cluster catalog out to arbitrarily high redshift. This catalog contains $N \gtrsim 30$ clusters at $z > 1$, providing the largest, mass-selected cluster sample at these redshifts. A dedicated study of this sample will help to place SPT-CL J2040−4451 in context with respect to the star-forming activity in the most massive high-redshift clusters.

The South Pole Telescope program is supported by the National Science Foundation through grant ANT-0638937. Partial support is also provided by the NSF Physics Frontier Center grant PHY-0114422 to the Kavli Institute of Cosmological Physics at the University of Chicago, the Kavli Foundation, and the Gordon and Betty Moore Foundation. Galaxy cluster research at Harvard is supported by NSF grant AST-1009012. Galaxy cluster research at SAO is supported in part by NSF grants AST-1009649 and MRI-0723073. The McGill group acknowledges funding from the National Sciences and Engineering Research Council of Canada, Canada Research Chairs program, and the Canadian Institute for Advanced Research. X-ray research at the CfA is supported through NASA Contract NAS 8-03060. The Munich group acknowledges support from the Excellence Cluster Universe and the DFG research program TR33. This work is based in part on observations obtained with the *Spitzer Space Telescope* (PID 60099), which is operated by the Jet Propulsion Laboratory, California Institute of Technology under a contract with NASA. Support for this work was provided by NASA through an award issued by JPL/Caltech. Additional data were obtained with the 6.5 m Magellan Telescopes located at the Las Campanas Observatory, Chile and the Blanco 4 m Telescope at Cerro Tololo Interamerican Observatories in Chile. R.J.F. is supported by a Clay Fellowship. B.A.B is supported by a KICP Fellowship, M. Bautz acknowledges support from contract 2834-MIT-SAO-4018 from the Pennsylvania State University to the Massachusetts Institute of Technology. M.D. acknowledges support from an Alfred P. Sloan Research Fellowship, W.F. and C.J. acknowledge support from the Smithsonian Institution. This research used resources of the National Energy Research Scientific Computing Center, which is supported by the Office of Science of the U.S. Department of Energy under contract No. DE-AC02-05CH11231. The authors also thank the referee, B. Lemaux, for his comments that improved the quality of this paper.

REFERENCES

Ashby, M. L. N., Stern, D., Brodwin, M., et al. 2009, ApJ, 701, 428
Autry, R. G., Probst, R. G., Starr, B. M., et al. 2003, Proc SPIIE, 4841, 525
Balogh, M. L., Morris, S. L., Yee, H. K. C., Carlberg, R. G., & Ellingson, E. 1997, ApJL, 488, L75
Beers, T. C., Flynn, K., & Gebhardt, K. 1990, AJ, 100, 32
Benson, B. A., de Haan, T., Dudley, J. P., et al. 2013, ApJ, 763, 147
Biviano, A., Durret, F., Gerbal, D., et al. 1996, A&A, 311, 95
Blanton, M. R., & Moustakas, J. 2009, ARA&A, 47, 159
Brodwin, M., Brown, M. J. I., Ashby, M. L. N., et al. 2006, ApJ, 651, 791
Brodwin, M., Gonzalez, A. H., Stanford, S. A., et al. 2012, ApJ, 753, 162
Brodwin, M., Ruel, J., Ade, P. A. R., et al. 2010, ApJ, 721, 90
Brodwin, M., Stanford, S. A., Gonzalez, A. H., et al. 2013, ApJ, 779, 138
Brodwin, M., Stern, D., Vikhlinin, A., et al. 2011, ApJ, 732, 33
Bruzual, G., & Charlot, S. 2003, MNRAS, 344, 1000
Carlberg, R. G., Yee, H. K. C., Ellingson, E., et al. 1997, ApJL, 476, L7

Carlstrom, J. E., Ade, P. A. R., Aird, K. A., et al. 2011, PASP, 123, 568
Carlstrom, J. E., Holder, G. P., & Reese, E. D. 2002, ARA&A, 40, 643
Chabrier, G. 2003, PASP, 115, 763
Colless, M., & Dunn, A. M. 1996, ApJ, 458, 435
De Lucia, G., & Blaizot, J. 2007, MNRAS, 375, 2
Dressler, A. 1980, ApJ, 236, 351
Dressler, A., & Gunn, J. E. 1983, ApJ, 270, 7
Duffy, A. R., Schaye, J., Kay, S. T., & Dalla Vecchia, C. 2008, MNRAS, 390, L64
Eisenhardt, P. R. M., Brodwin, M., Gonzalez, A. H., et al. 2008, ApJ, 684, 905
Elston, R. J., Gonzalez, A. H., McKenzie, E., et al. 2006, ApJ, 639, 816
Evrard, A. E., Bialek, J., Busha, M., et al. 2008, ApJ, 672, 122
Fassbender, R., Böhringer, H., Nastasi, A., et al. 2011, NJPh, 13, 125014
Fazio, G. G., Hora, J. L., Allen, L. E., et al. 2004, ApJS, 154, 10
Foley, R. J., Andersson, K., Bazin, G., et al. 2011, ApJ, 731, 86
Gettings, D. P., Gonzalez, A. H., Stanford, S. A., et al. 2012, ApJL, 759, L23
Gifford, D., Miller, C., & Kern, N. 2013, ApJ, 773, 116
Girardi, M., Fadda, D., Giuricin, G., et al. 1996, ApJ, 457, 61
Gonzalez, A. H., Brodwin, M., Brown, M. J. I., et al. 2010, BAAS, 216, 415.13
Goto, T. 2005, MNRAS, 359, 1415
Hamuy, M., Suntzeff, N. B., Heathcote, S. R., et al. 1994, PASP, 106, 566
Hasselfield, M., Hilton, M., Marriage, T. A., et al. 2013, JCAP, 07, 008
High, F. W., Stubbs, C. W., Rest, A., Stalder, B., & Challis, P. 2009, AJ, 138, 110
Hilton, M., Stanford, S. A., Stott, J. P., et al. 2009, ApJ, 697, 436
Holden, B. P., van der Wel, A., Franx, M., et al. 2005, ApJL, 620, L83
Hopkins, P. F., Hernquist, L., Cox, T. J., & Kereš, D. 2008, ApJS, 175, 356
Hu, W., & Kravtsov, A. V. 2003, ApJ, 584, 702
Kennicutt, R. C., Jr. 1998, ARA&A, 36, 189
Komatsu, E., Smith, K. M., Dunkley, J., et al. 2011, ApJS, 192, 18
Koranyi, D. M., & Geller, M. J. 2000, AJ, 119, 44
Lemaux, B. C., Lubin, L. M., Shapley, A., et al. 2010, ApJ, 716, 970
Lotz, J. M., Papovich, C., Faber, S. M., et al. 2013, ApJ, 773, 154
Mancone, C. L., Baker, T., Gonzalez, A. H., et al. 2012, ApJ, 761, 141
Mancone, C. L., Gonzalez, A. H., Brodwin, M., et al. 2010, ApJ, 720, 284
Marriage, T. A., Acquaviva, V., Ade, P. A. R., et al. 2011, ApJ, 737, 61
McLeod, B., Geary, J., Ordway, M., et al. 2006, in Scientific Detectors for Astronomy 2005, ed. J. E. Beletic, J. W. Beletic, & P. Amico (Berlin: Springer), 337
Mei, S., Holden, B. P., Blakeslee, J. P., et al. 2006, ApJ, 644, 759
Mohr, J. J., Geller, M. J., & Wegner, G. 1996, AJ, 112, 1816
Mullis, C. R., Rosati, P., Lamer, G., et al. 2005, ApJL, 623, L85
Muzzin, A., Wilson, G., Demarco, R., et al. 2013, ApJ, 767, 39
Muzzin, A., Wilson, G., Yee, H. K. C., et al. 2009, ApJ, 698, 1934
Navarro, J. F., Frenk, C. S., & White, S. D. M. 1997, ApJ, 490, 493
Oemler, A., Jr. 1974, ApJ, 194, 1
Papovich, C., Momcheva, I., Willmer, C. N. A., et al. 2010, ApJ, 716, 1503
Pimbblet, K. A., Smail, I., Edge, A. C., et al. 2006, MNRAS, 366, 645
Planck Collaboration, Ade, P. A. R., Aghanim, N., et al. 2013, arXiv:1303.5080
Reichardt, C. L., Stalder, B., Bleem, L. E., et al. 2013, ApJ, 763, 127
Rest, A., Stubbs, C., Becker, A. C., et al. 2005, ApJ, 634, 1103
Rosa-González, D., Terlevich, E., & Terlevich, R. 2002, MNRAS, 332, 283
Rosati, P., Tozzi, P., Ettori, S., et al. 2004, AJ, 127, 230
Rosati, P., Tozzi, P., Gobat, R., et al. 2009, A&A, 508, 583
Rudnick, G. H., Tran, K.-V., Papovich, C., Momcheva, I., & Willmer, C. 2012, ApJ, 755, 14
Ruel, J., Bazin, G., Bayliss, M., et al. 2014, ApJ, 792, 45
Santos, J. S., Tozzi, P., & Rosati, P. 2011, MSAIS, 17, 66
Shapley, A. E., Steidel, C. C., Pettini, M., & Adelberger, K. L. 2003, ApJ, 588, 65
Skrutskie, M. F., Cutri, R. M., Stiening, R., et al. 2006, AJ, 131, 1163
Snyder, G. F., Brodwin, M., Mancone, C. M., et al. 2012, ApJ, 756, 114
Song, J., Zenteno, A., Stalder, B., et al. 2012, ApJ, 761, 22
Stalder, B., Ruel, J., Šuhada, R., et al. 2013, ApJ, 763, 93
Stanford, S. A., Brodwin, M., Gonzalez, A. H., et al. 2012, ApJ, 753, 164
Stanford, S. A., Eisenhardt, P. R., Brodwin, M., et al. 2005, ApJL, 634, L129
Stanford, S. A., Eisenhardt, P. R., & Dickinson, M. 1998, ApJ, 492, 461
Stanford, S. A., Romer, A. K., Sabirli, K., et al. 2006, ApJL, 646, L13
Staniszewski, Z., Ade, P. A. R., Aird, K. A., et al. 2009, ApJ, 701, 32
Sunyaev, R. A., & Zel'dovich, Y. B. 1972, CoASP, 4, 173
Tran, K.-V. H., Papovich, C., Saintonge, A., et al. 2010, ApJL, 719, L126
Vanderlinde, K., Crawford, T. M., de Haan, T., et al. 2010, ApJ, 722, 1180
Weiner, B. J., Coil, A. L., Prochaska, J. X., et al. 2009, ApJ, 692, 187
Williamson, R., Benson, B. A., High, F. W., et al. 2011, ApJ, 738, 139
Yan, R., & Blanton, M. R. 2012, ApJ, 747, 61
Yan, R., Newman, J. A., Faber, S. M., et al. 2006, ApJ, 648, 281
Zeimann, G. R., Stanford, S. A., Brodwin, M., et al. 2012, ApJ, 756, 115